Journal of the Physical Society of Japan
Vol. 66, No. 12, December, 1997, pp. 3795-3800

Characteristics of the Tokyo Electron-Beam Ion Trap

Hirofumi WATANABE[1,2,*], Junji ASADA[2], Frederick John CURRELL[2], Tsunemitsu FUKAMI[2], Takato HIRAYAMA[3], Kenji MOTOHASHI[4], Nobuyuki NAKAMURA[5], Eimitsu NOJIKAWA[5], Shunsuke OHTANI[2,5], Kiyohiko OKAZAKI[6], Makoto SAKURAI[7], Hiroshi SHIMIZU[2], Naoko TADA[5] and Seiji TSURUBUCHI[4]

[1] *Kyoto University Faculty of Engineering, Kyoto, Kyoto 606-01*
[2] *University of Electro-Communications Institute for Laser Science, Chofu, Tokyo 182*
[3] *Gakushuin University Faculty of Science, Toshima, Tokyo 171*
[4] *Tokyo University of Agriculture and Technology Faculty of Technology, Koganei, Tokyo 184*
[5] *Japan Science and Technology Corporation, Chofu, Tokyo 182*
[6] *Institute of Physical and Chemical Research (Riken), Wako, Saitama 351*
[7] *Institute for Molecular Science, Okazaki, Aichi 444*

(Received August 15, 1997)

We have constructed a new Electron Beam Ion Trap (EBIT). Over recent months, we have operated this device and obtained some experimental results. In this paper, we show the performance of this EBIT by illustrating these results.

KEYWORDS: ion trap, EBIT, highly charged ions, ion source, X-ray spectra

§1. Introduction

The electron beam ion trap (EBIT) is a unique ion source as a means of producing and trapping highly charged ions, which was developed initially at Lawrence Livermore National Laboratory (LLNL) for spectroscopic studies.[1)] It is based on the electron beam ion source (EBIS) concept,[2)] but with a shorter trap length to limit plasma instability.

Several EBITs have been constructed throughout the world.[3-5)] Most of the EBITs have similar operation parameters with an electron beam energy of up to 30 keV. For highly stripped ions of high-Z atoms, the electron impact ionization cross sections increase gradually with the electron energy.[6)] Therefore a high energy electron beam is favorable for producing high-Z ions with very high-charge states. In LLNL, a high-energy EBIT with a maximum energy of 210 keV has been developed,[7)] where bare uranium ions could be produced.[8)]

We have constructed a new EBIT at the University of Electro-Communications, Tokyo, which is designed to generate a 340 keV, 300 mA electron beam. The structure and the details of this EBIT (the Tokyo EBIT) have been illustrated in previous papers.[9-12)] In this report, we introduce some experimental results related to the performance of the Tokyo EBIT.

§2. An Overview of the Tokyo EBIT

A schematic drawing of the Tokyo EBIT is shown in Fig. 1. In the lower part, there is an electron gun. In the upper part, there is an electron collector. In between these sections, there is a drift tube assembly in which ions are trapped. This assembly is comprised of three successive cylindrical electrodes, which produce an axial trapping potential due to the positive potential applied to the end drift tubes with respect to the central one. Eight ports surround the central drift tube. These ports are used for observations, neutral gas injection and laser introduction. Liquid helium and liquid nitrogen tanks are situated around and over the trap assembly. They act as cryo-pumps to evacuate the trap region. A super-

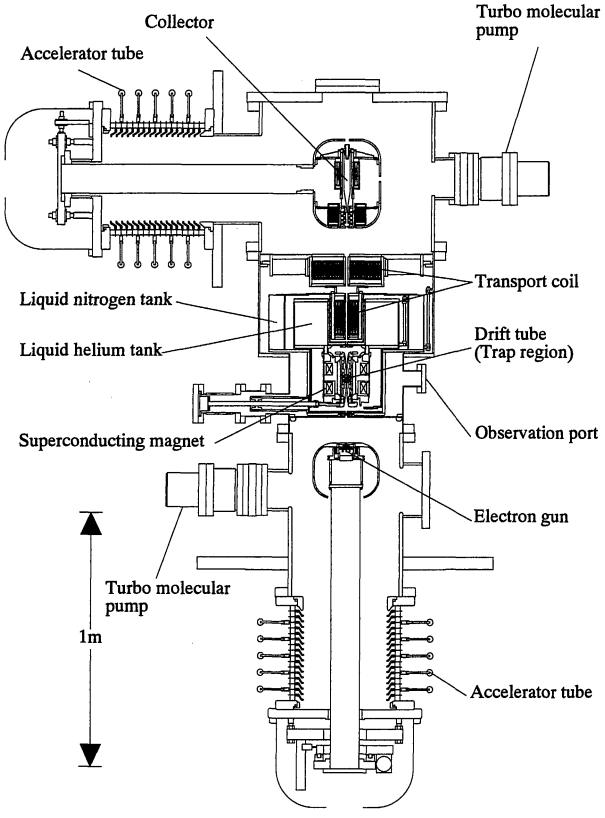

Fig. 1. Schematic drawing of the Tokyo EBIT.

* E-mail: h_watana@ils.uec.ac.jp

Table I. The operational parameters of different EBITs.

Parameter	EBIT2[13]	Super-EBIT[13]	Tokyo-EBIT (designed)[a]	Tokyo-EBIT (achieved)
Beam Energy (keV)	0.5–30	10–210	10–340	2.5–80
Beam Current (mA)	0–200	0–200	0–300	0–250
Magnetic field (T)	0–3	0–3	0–4.5	0–4.5
Electron Beam Radius (μm)	35	35	$\leq$30	<85[b]

a) While the electrical potential applied to Tokyo EBIT is designed to be 340 eV, now we can apply up to 100 kV. This is because the insulation voltage of the outside of the EBIT is 100 kV. When we operate over 100 kV, SF_6 gas will be used for insulation.
b) This value was obtained by the visible CCD camera. This value gives an upper limit of the diameter. The details are given in the text.

conducting coil is installed in the liquid helium tank to generate a magnetic field which compresses the electron beam.

The electrons emitted from the cathode are accelerated upwards by the potential difference between the electron gun and the drift tubes, whilst being magnetically compressed. The resultant beam ionizes and traps ions at the drift tubes. After exiting the drift tubes, the electron beam is decelerated by the potential difference between the drift tubes and the collector, and then collected by the electron collector. Both the electron gun and the electron collector assemblies are designed to be floated to -300 kV, and the drift tube assembly is to $+40$ kV from laboratory earth. Therefore it is possible to generate an electron beam with an energy of up to 340 keV at the trap region.

The design parameters of the Tokyo EBIT are listed in Table I together with operational parameters which have been achieved. In this table the main parameters of the other EBITs[13] are also listed. A maximum beam energy of 80 keV and a maximum current of 250 mA have been achieved. While the Tokyo EBIT is designed to generate a 340 keV electron beam, now we can apply an accelerating voltage to the EBIT of up to 100 kV. This is because the isolation voltage of the outside of the Tokyo EBIT is 100 kV. When we operate over 100 kV, SF_6 gas will be used.

§3. Measured Properties of the Tokyo EBIT

3.1 The electron gun

The electron gun of the Tokyo EBIT is a pierce-type, which consists of cathode, focus, anode and snout electrodes. Extensive computer simulation of the electron beam trajectory has been performed using "EGUN2"[14] to optimize the structure of the electron gun. A typical result is displayed in Fig. 2.

In Fig. 3 the anode voltage dependence of the electron beam current and the predicted dependence (derived from the design value of the perveance of 4×10^{-6} A/V$^{3/2}$) are shown. This figure shows that the measured values follow the calculated curve. This result shows that the electron gun is working as expected.

The cathode is a spherical-concave shaped dispenser-type cathode, which is a porous tungsten matrix infiltrated with BaO, CaO and Al_2O_3. The diameter of this cathode is 3 mm. The work function of the cathode materials is reduced by Os and Ru put over the surface of the cathode to reduce the temperature at which it

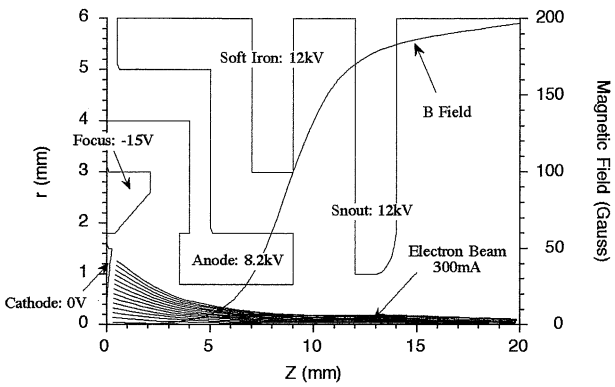

Fig. 2. A computer simulation of the electron beam trajectories in the electron gun.

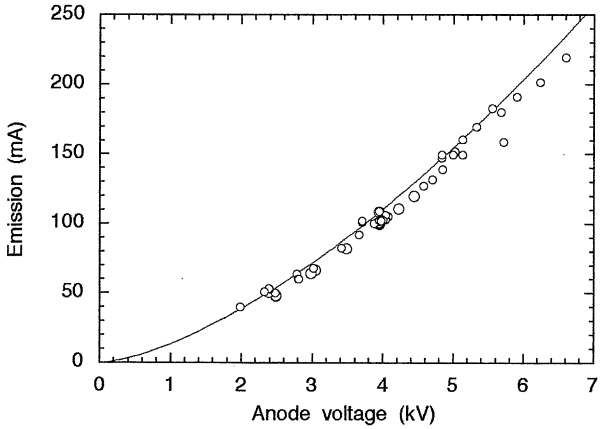

Fig. 3. The beam current dependence on the voltage applied to the anode electrode.

works. The designed value of the maximum current output is 300 mA. Now we have achieved 250 mA at 75 keV electron beam energy, which is about 83% of the design value.

3.2 The image of the electron beam

It is known that the highly charged ions in the EBIT emit light in the visible region, and visible spectra have been observed.[15,16] The electron beam profile at the trap region was measured by a visible CCD camera. The result of this measurement is shown in Fig. 4, taken when using a 20 keV, 150 mA electron beam. Xe gas was injected from an observation port. The straight line surrounded by the slit image is the image of the electron

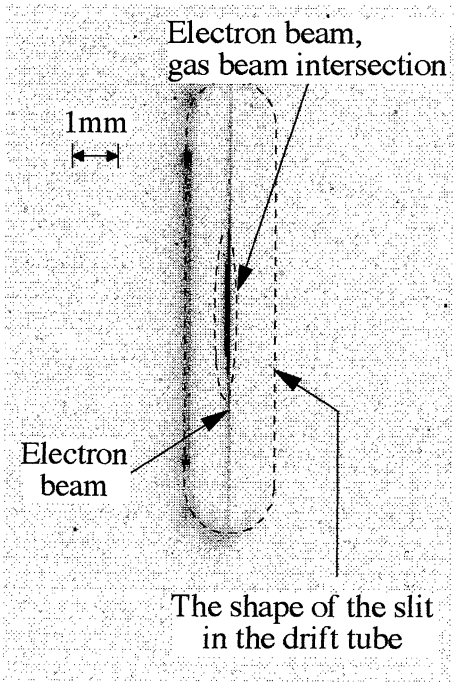

Fig. 4. The electron beam profile image at the drift tube, as measured with a visible CCD camera.

beam. There is a dark region in the center of the electron beam image, which is due to the crossing of the electron beam with the neutral Xe gas beam. Since the precise focusing of the camera is difficult and light is sometimes emitted outside of the electron beam due to ions with long lived excited states which decay in the visible, this measurement gives the upper limit of the electron beam radius. The intensity distribution of the beam image was fitted by a Gaussian function, and the full width at half maximum was 110 μm. This gives an 80% beam radius of about 85 μm.

3.3 Overcooling

There is a liquid helium tank around and over the trap region. In the lower part of this tank (called the "coil vessel") a superconducting Helmholtz coil is installed. About 14 l of liquid helium can be stored, which is consumed in about seven hours. The coil vessel also works as a cryo-pump and evacuates the trap region. The quality of vacuum attained in the trap determines the charge balance obtained in the trap. The superconducting coil and trap region are normally at 4.2 K.

The liquid helium is dropped through a Joule-Thompson valve into a tube installed at the top in the coil vessel. This tube is evacuated by a rotary pump, through a flow control valve. The dropped liquid helium is adiabatically expanded and cools the tube, by the Joule-Thompson effect. The liquid helium in the vessel is cooled through this tube, resulting in the whole trap region being cooled to below 2.4 K. At a temperature of around 4.2 K, it is considered that the vacuum is dominated by hydrogen molecules and helium atoms. Since if the temperature falls from 4.2 K to 2.4 K, the vapor pressure of hydrogen molecules is less than 10^{-15} Torr.[17] Therefore by overcooling, the vacuum in the trap region will be improved, leading to a reduction in the charge exchange rate.

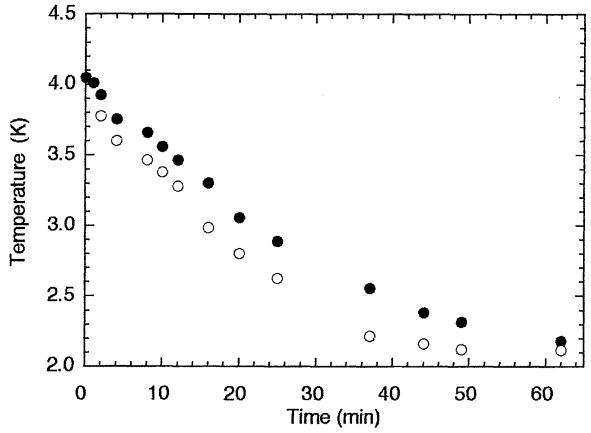

Fig. 5. Temperature variation as a function of time after the start of the overcooling procedure. • and ○ are temperatures measured at the top and the bottom of the coil vessel respectively.

The time variation in the temperature was measured by two resistance thermometers (LakeShore Carbon Glass Resistor model no. CGR-1-500) situated at the top and bottom of the coil vessel. The result is shown in Fig. 5. It can be seen that by about 30 minutes after the start of the overcooling procedure the temperature becomes 2.4 K. The trap region is overcooled to below 2.4 K.

3.4 The beam monitor

To monitor the electron beam trajectory, two capacitive beam monitors[18] are situated at the front and back of the trap region. Each capacitive beam monitor is four electrodes in a square configuration. When the electron beam current is modulated by a small portion, the induced charge on the electrodes changes. Since the magnitude of the induced charge depends on the distance of the electron beam from the electrode, the difference of the charge which is induced on an opposite pair of electrodes is related to the position of the electron beam between the pair of electrodes.

A typical output from the capacitive beam-monitor is shown in Fig. 6. The upper capacitive monitor (i.e. after the trap) was used for this measurement. The electron beam energy was 20 keV and the electron beam current was modulated between 50 mA and 48 mA. Synchronized with the modulation of the electron beam current, the differences of the voltage induced at the pairs of the electrodes were observed. Since, if the electron beam passes through the center axis between the monitor electrodes, no signal will be observed, the position of the electron beam is off-center between the monitor electrodes. A detailed design of this beam monitor will be given in the near future.[19]

3.5 Radiative recombination spectrum

Figure 7 shows an X-ray spectrum measured with a Ge solid state detector. The electron beam energy and current in this measurement were 75 keV and 150 mA respectively. Krypton gas was introduced from an obser-

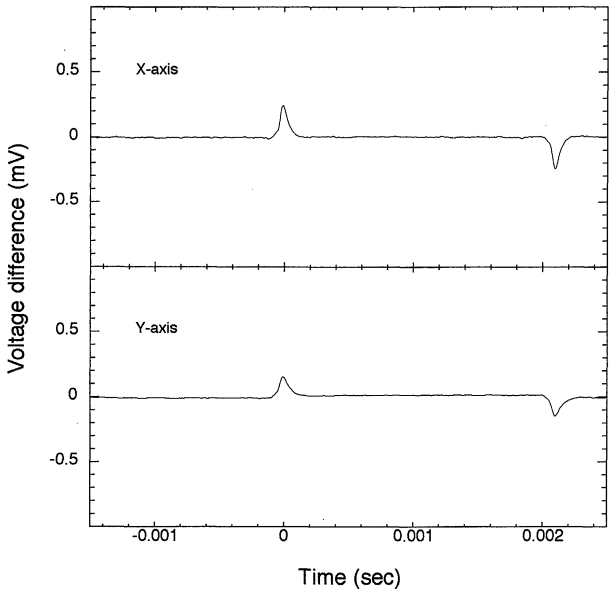

Fig. 6. The signal from a capacitive beam monitor. The voltage difference induced on the monitor electrodes, synchronized with the electron beam current modulation.

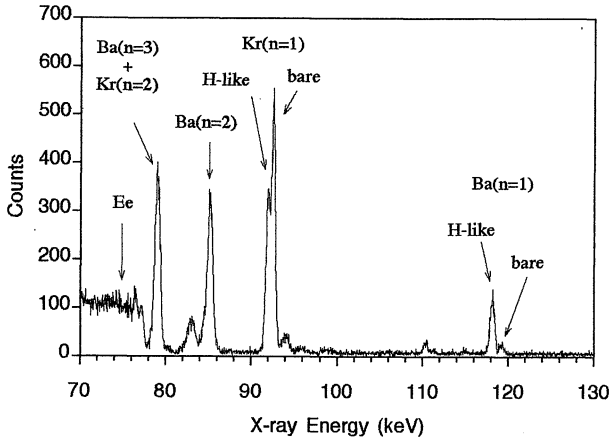

Fig. 7. A radiative recombination spectrum of Kr and Ba ions. Details are given in the text.

vation port of the EBIT. Radiative recombination (RR) lines of highly charged barium and krypton ions were observed. The source barium is evaporated from the cathode, subsequently ionized and trapped. The small peaks observed at 83 and 94 keV are from RR into the highly charged tungsten ions which also originate from the cathode.

The bremsstrahlung radiation continues up to the electron beam energy. RR lines appear at energies above the bremsstrahlung radiation, since the energy of an RR line is the sum of the electron beam energy and the ionization energy of the captured electron. The RR lines observed are to the $n = 1$, $n = 2$ and $n = 3$ levels of Ba and Kr ions, converging to the continuum of bremsstrahlung radiation. RR lines to $n = 1$ level split into two peaks for Ba and Kr ions. The peak at the higher energy side is from RR into bare ions, and that at the lower side is from RR into H-like ions. This spectrum shows the production of bare barium ions (Ba^{56+} ions) in the trap.

For Ba, the peak for RR into bare ions is smaller than that for RR into H-like ions, while for Kr the situation is reversed. This indicates that the charge balance of Kr ions is much better than Ba ions. The energy which is needed to remove the final electron is 43 keV for Ba and 17 keV for Kr, while the electron beam energy is 75 keV. Therefore the electron beam energy is 4.4 times the ionization energy of H-like Kr and 1.7 times that of H-like Ba ions. The electron impact ionization cross section of H-like Kr is large enough to produce more bare ions than H-like ones.

3.6 Dielectronic recombination

When a free electron is captured into the bound state of ions and simultaneously a bound electron is excited, doubly excited ions are produced. This is the inverse process of the Auger process. When such an ion decays by photon emission, the process is called dielectronic recombination (DR). Knapp *et al.* obtained a two-dimensional X-ray spectrum by ramping the electron beam energy linearly,[20] measuring the X-ray signed as a function of the electron beam energy. In this measurement the ramping speed was fast enough, so the charge balance in the trap remained almost constant. In their spectrum, DR processes were observed when the electron beam energy matched the resonant energies.

We have also measured two-dimensional X-ray spectra[21] using a multiparameter system.[22] The result of this type of measurement is shown in Fig. 8. In this figure the vertical axis indicates the electron beam energy, and the horizontal axis the X-ray energy. The details of this measurement will be described elsewhere.[23] Here, we introduce the outline of this spectrum.

In this measurement krypton gas was introduced from the outside of the EBIT. The electron beam current was 100 mA. The electron beam energy to produce the initial charge state distribution was 17 keV, which is almost identical to the ionization energy of He-like Kr ions (16.8 keV) and is much larger than that of Li-like Kr ions (4 keV). Therefore, it can be considered that He-like Kr ions were predominant in the trap. The electron beam energy was ramped linearly from 17 keV to 7 keV and then from 7 keV to 17 keV. This ramp was performed once per 100 ms and its width was 20 ms. X-rays emitted by highly charged ions were measured by the Ge solid state detector.

In Fig. 8, the darkness reveals the strength of the X-ray intensity. In the area at the left side of this figure, where the X-ray energy is lower than the beam energy, there is a dark area which is attributed to the bremsstrahlung radiation. On this area, vertical lines appear, which are the bound-bound transitions of Kr ions. The line at around 13 keV X-ray energy comes from the $n = 2$–1 transitions, and that at around 15.5 keV comes from $n = 3$–1 transitions. Diagonal lines are attributed to RR lines, since the X-ray energy of the RR lines increases linearly with the electron beam energy. The RR lines to $n = 2$ and $n = 3$ levels clearly appear. At the crossings of the vertical and diagonal lines, there are dark spots. These are due to DR of He-like Kr ions. Identification of these spots is noted on the figure.

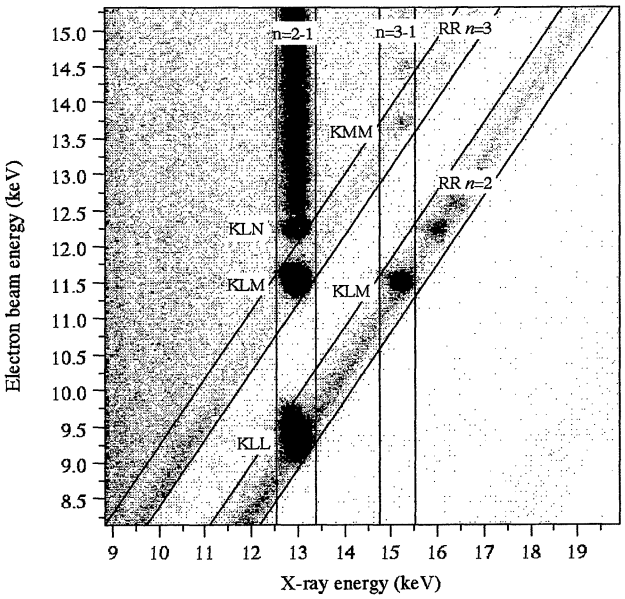

Fig. 8. A two dimensional X-ray spectrum of Kr ions. The vertical axis is the electron beam energy and the horizontal axis is the X-ray energy, in keV. The darkness in the figure reveals the X-ray count.

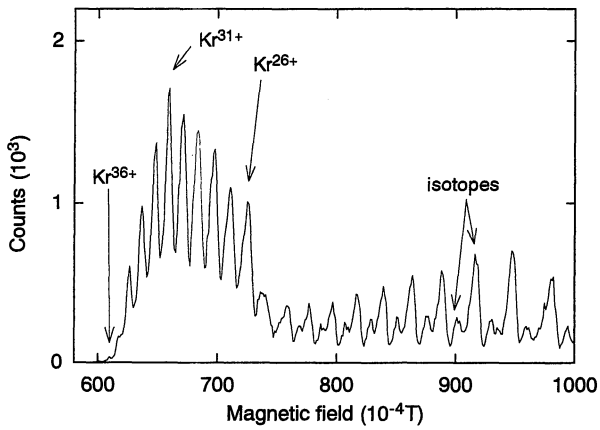

Fig. 9. A mass spectrum of krypton ions. This spectrum was obtained using a pulsed extraction mode, but also has contributions from continuous extraction, as described in the main text. The electron beam energy was 27.6 keV and the current was about 110 mA.

3.7 Charge distribution of extracted ions

The Tokyo EBIT has a beam line for extraction of trapped ions, to facilitate ion-surface experiments. The details of this beam line have been outlined in a previous paper.[12] Here, we show a mass spectrum of highly charged krypton ions obtained using the Tokyo EBIT. In this measurement, krypton gas was introduced from an observation port. Ions were extracted by a pulsed extraction mode, where the potential of the central drift tube (DT2) is set to the same potential as the upper drift tube (DT3) to dump the trapped ions. During dumping, the potential of DT2 was linearly changed from +2.6 kV to +2.7 kV with respect to laboratory earth during 20 ms, and then returned to +2.6 kV rapidly. This procedure was performed three times per second. It is considered that the charge distribution measured during the pulsed extraction reflects the charge balance in the trap. This is in contrast with continuous extraction, where only ions traveling over the potential wall of the upper drift tube are extracted. The potential of DT3 was fixed to be +2.7 kV and that of the lower drift tube (DT1) to be +2.8 kV with respect to laboratory earth. Since the potential of DT3 was +2.7 kV, the extracted ions have an energy of $2.7q$ keV, where q is the charge state of the extracted ions. During trapping, the electron beam energy was set to be 27.6 keV and the current was about 110 mA. The extracted ions were analyzed by a sector magnet, multiplied by a microchannel plate, and then counted. The counts were accumulated for one second at every data point. Therefore, each point contains fractions of both the continuous and pulsed extraction modes. The result is shown in Fig. 9. There is a peak in the charge state distribution at higher charge states, and the maximum is at Kr^{31+}. In this spectrum a small fraction of bare-Kr ions are observed.

In Fig. 10, the time variation in detected intensity is shown for specific charge states, that is, Kr^{30+} ions (a), Kr^{20+} ions (b) and Kr^{6+} ions (c). All of these spectra have similar structure. After an initial onset, there is a region of almost constant intensity followed by a sharp peak. This pattern repeats, synchronized with the dumping process. The constant part is the contribution from continuous extraction, while the peaked part is from pulse extraction. Thus the constant part reflects the escaping ions, while the peaked part reflects the number of trapped ions. The ions which have an energy greater than qeV can escape from the trap, where V is the axial trapping potential, q the charge state of ions and e the elementary electric charge. All ions in thermal equilibrium have almost the same temperature, while the height of the potential barrier is different. depending on the charge state of the ions. Therefore lower charge state ions escape more easily. Thus the intensity ratio of the continuous part to the peaked part for lower charge state ions is larger than that for higher charge state ions.

From these observations, the intensity of lower charge state ions in the mass spectrum in Fig. 9 does not reflect the number of the trapped ions, while that of higher charge state ions comes from the trapped ions. Moreover, the axial escape rate of the higher charge state ions is almost negligible.

§4. Conclusion

We have designed and constructed a new EBIT, which is now in operation. This EBIT has novel properties such as a high emissivity cathode, overcooling, and capacitive beam monitors. The device is now being run routinely, producing new data as we have illustrated here.

Acknowledgment

The authors are grateful for the Grant-in-Aid for Scientific Research on the priority area "Atomic Physics of Multicharged Ions", from the Ministry of Education, Science and Culture. The main part of the Tokyo EBIT was constructed by Sumitomo Heavy Industries, Ltd. Tokyo Cathode Laboratory, Ltd. has provided the newly devel-

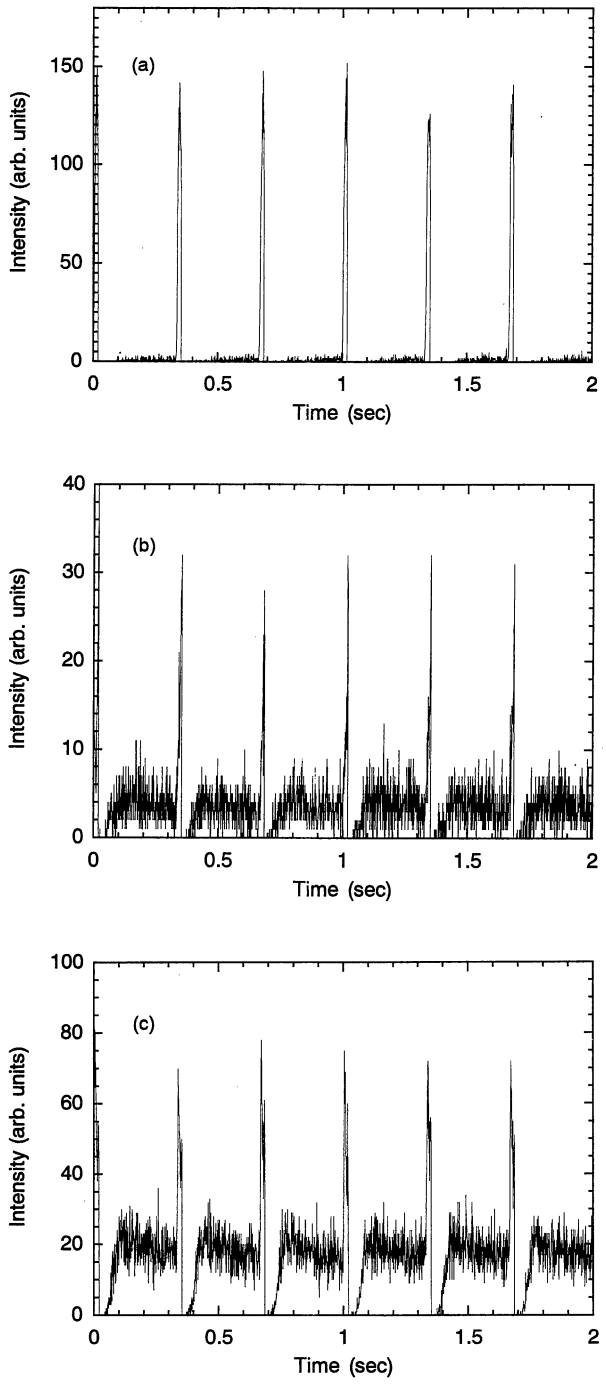

Fig. 10. The time variation in intensity of the extracted ions. (a) is Kr^{30+} ions, (b) Kr^{20+} ions and (c) Kr^{6+} ions.

oped cathodes. We thank the engineers in these companies for their useful discussions. We also thank Ann Currell for help in preparing this manuscript. Finally, we are also grateful to Kazuo Nishizawa for his great contribution to the completion of the Tokyo EBIT in our laboratory.

1) M. A. Levine, R. E. Marrs, J. R. Henderson, D. A. Knapp and M. B. Schneider: Phys. Scr. T **22** (1988) 157.
2) E. D. Donets and V. P. Ovsyannikov: Sov. Phys.-JETP **53** (1981) 466.
3) J. D. Silver, A. J. Varney, H. S. Margolis, P. G. E. Baird, I. P. Grant, P. D. Groves, W. A. Hallet, A. T. Handford, P. J. Hirst, A. R. Holmes, D. J. H. Howie, R. A. Hunt, K. A. Nobbs, M. Roberts, W. Studholme, J. S. Wark, M. T. Williams, M. A. Levine, D. D. Dietrich, W. G. Graham, I. D. Williams, R. O' Neil and S. J. Rose: Rev. Sci. Instrum. **65** (1994) 1072.
4) J. D. Gillaspy, Y. Aglitskiy, E. W. Bell, C. M. Brown, C. T. Chantler, R. D. Deslattes, U. Feldman, L. T. Hudson, J. M. Laming, E. S. Meyer, C. A. Morgan, A. I. Pikin, J. R. Roberts, L. P. Ratliff, F. G. Serpa, J. Sugar and E. Takács: Phys. Scr. T **59** (1995) 392.
5) C. Biedermann, A. Föster, G. Fußmann and R. Radtke: Phys. Scr. T **73** (1997) 360.
6) D. L. Moores and K. J. Reed: Nucl. Instrum. Methods B **98** (1995) 122.
7) D. A. Knapp, R. E. Marrs, S. R. Elliot, E. W. Magee and R. Zasadzinski: Nucl. Instrum. Methods A **334** (1993) 305.
8) R. E. Marrs, S. R. Elliott and D. A. Knapp: Phys. Rev. Lett. **72** (1994) 4082.
9) F. J. Currell, J. Asada, K. Ishii, A. Minoh, K. Motohashi, N. Nakamura, K. Nishizawa, S. Ohtani, K. Okazaki, M. Sakurai, H. Shiraishi, S. Tsurubuchi and H. Watanabe: J. Phys. Soc. Jpn. **65** (1996) 3186.
10) N. Nakamura, J. Asada, F. J. Currell, T. Fukami, T. Hirayama, K. Motohashi, T. Nagata, E. Nojikawa, S. Ohtani, K. Okazaki, M. Sakurai, H. Shiraishi, S. Tsurubuchi and H. Watanabe: Phys. Scr. T **73** (1997) 362.
11) H. Watanabe, J. Asada, F. J. Currell, T. Fukami, T. Hirayama, K. Motohashi, N. Nakamura, E. Nojikawa, S. Ohtani, K. Okazaki, M. Sakurai, H. Shiraishi and S. Tsurubuchi: Phys. Scr. T **73** (1997) 365.
12) K. Motohashi, J. Asada, F. J. Currell, T. Fukami, T. Hirayama, K. Mochiji, N. Nakamura, E. Nojikawa, K. Okazaki, S. Ohtani, M. Sakurai, H. Shiraishi, S. Tsurubuchi and H. Watanabe: Phys. Scr. T **73** (1997) 368.
13) S. R. Elliott: Nucl. Instrum. Methods B **98** (1995) 114.
14) W. B. Hermannsfeldt: Phys. Scr. T **71** (1997) 28.
15) C. A. Morgen, F. G. Serpa, E. Takács, E. S. Meyer, J. D. Gillaspy, J. Sugar, J. R. Roberts, C. M. Brown and U. Feldman: Phys. Rev. Lett. **74** (1995) 1716.
16) F. G. Serpa, E. W. Bell, E. S. Meyer, J. D. Gillaspy and J. R. Roberts: Phys. Rev. A **55** (1997) 1832.
17) *Lehrgranshandbuch Kryotechnik* (Verein Deutscher Ingenieure, Berlin, 1977).
18) F. J. Currell, J. Asada, K. Ishii, K. Motohashi, N. Nakamura, K. Nishizawa, S. Ohtani, K. Okazaki, M. Sakurai, S. Tsurubuchi and H. Watanabe: *Proc. 19th ICPEAC, Whistler, 1995*, Vol. 2, p. 798.
19) J. Asada, F. J. Currell, T. Fukami, T. Hirayama, K. Motohashi, N. Nakamura, E. Nojikawa, S. Ohtani, K. Okazaki, M. Sakurai, S. Tsurubuchi and H. Watanabe: in preparation.
20) D. A. Knapp: Z. Phys. D **21** (1991) S143.
21) J. Asada, F. J. Currell, T. Fukami, T. Hirayama, K. Motohashi, N. Nakamura, E. Nojikawa, S. Ohtani, K. Okazaki, M. Sakurai, H. Shiraishi, S. Tsurubuchi and H. Watanabe: Phys. Scr. T **73** (1997) 90.
22) F. J. Currell, J. Asada, T. Fukami, T. Hirayama, N. Nakamura, K. Motohashi, E. Nojikawa, K. Okazaki, S. Ohtani, M. Sakurai, H. Shiraishi, S. Tsurubuchi and H. Watanabe: Phys. Scr. T **73** (1997) 371.
23) J. Asada, F. J. Currell, T. Fukami, T. Hirayama, K. Motohashi, N. Nakamura, E. Nojikawa, S. Ohtani, K. Okazaki, M. Sakurai, S. Tsurubuchi and H. Watanabe: in preparation.